Dynamical Climatology

Rossby wavetrains in the stratosphere forced by localised disturbances in the troposphere.

by

C.J. Marks, A. O'Neill and V.D. Pope

DCTN 15 January 1985

Meteorological Office (Met. O. 20)
London Road
Bracknell
Berkshire RG12 2SZ

DYNAMICAL CLIMATOLOGY TECHNICAL NOTE NO. 15

ROSSBY WAVETRAINS IN THE STRATOSPHERE FORCED BY LOCALISED DISTURBANCES IN THE TROPOSPHERE

by

C J Marks

Department of Atmospheric Physics, Clarendon Laboratory, Parks Road, Oxford, U.K.

A O'Neill

V D Pope

This paper has been submitted for publication in the Proceedings of the Workshop on the Dynamics of Long Waves in the Atmosphere, Kristineberg, Sweden, 24-26 August 1984.

Met O 20 (Dynamical Climatology Branch)
Meteorological Office
London Road
Bracknell
Berkshire, U.K. RG12 2SZ

January 1985

Abstract

We examine the structure and propagation of disturbances in the stratosphere that originate from localised sources in the troposphere. A comparison of the effects of both small and large amplitude forcing is presented, and regions where non-linear processes are important are thus located. Wave breaking is clearly exhibited by the large-amplitude wavetrains. This is inferred from isentropic maps of Ertel's potential vorticity which are used to study the evolution of the phenomenon.

Section 1: Introduction

There have been a number of studies which have linked elements of the stratospheric circulation with particular, localised features of the tropospheric circulation. In an analytical study, Hayashi(1981) has proposed that the persistent 'Aleutian High' in the winter stratosphere is mainly a downstream response to the dominant 'East Asian Low' at mid latitudes in the troposphere. Observational studies have noted an association between blocking in the troposphere and the so-called sudden warming in the stratosphere (e.g. O'Neill and Taylor, 1979). These findings suggest a study of the response of the stratosphere to forcing by localised disturbances in the troposphere. This is the purpose of the present work.

We use a multi-level, primitive equation model of the stratosphere and mesosphere, the height of whose lower boundary in the troposphere can be prescribed. Localised disturbances which grow to steady amplitude are applied at this lower boundary and the response of the initially axially symmetric atmosphere is studied. Hitherto, most idealised perturbation experiments designed to investigate the forcing effect of the troposphere on the stratosphere have used an applied disturbance restricted to zonal harmonic wavenumber 1 or 2 (e.g. Holton,1976 ;Butchart et al.,1982). The implicit assumption is made that an increase of a particular zonal harmonic in the stratosphere is driven by a corresponding increase of that harmonic in the troposphere. When the dynamics are strongly non-linear this need not be the case, which is the reason the response to different types of idealised forcing should be investigated. We therefore regard our

experiments as complementing rather than replacing the simulations with simple harmonic forcing. We note, however, that there is no known mechanism which selectively favours the growth of wave 1 or wave 2 in the troposphere over periods of a week or so when marked changes in the stratospheric circulation can occur. It seems likely instead that any rapid fluctuations in the amplitudes and phases of wave 1 or wave 2 in the troposphere are the complicated signature of comparatively localised changes in the circulation. On the other hand, the analytically prescribed forcing that we apply is also idealised. The value of both types of experiment must be determined by their ability to reproduce observed aspects of the circulation in the upper atmosphere.

A comparison of our results with observations is beyond the scope of our brief account here and is reserved for a fuller version of the paper, in preparation. Our present aims are as follows. Firstly, we note some properties of Rossby wavetrains which emanate from local sources in the troposphere and propagate upwards and downstream into the stratosphere. We point to the properties of the basic state of the atmosphere which influence this propagation and the wave structure. Ideally, results should be compared for a range of basic states. For brevity, we confine attention here to propagation on only one zonally symmetric state, chosen to illustrate a number of interesting features of wave dynamics. A comparison of results for different basic states is included in the fuller version of the paper.

A central theme of our study is a comparison between the responses to disturbances of small and large amplitude, in order to examine their differing behaviour and to locate regions where

non-linear processes are important. Regions where waves 'break' are shown to be where the strongest non-linearities arise. For stationary forcing, this happens in the vicinity of zero-wind lines ('critical lines',see McIntyre,1982; Warn and Warn,1976). The evolution of wave breaking is followed using isentropic maps of Ertel's potential vorticity, which allow the movement of material to be followed insofar as inviscid, adiabatic conditions apply.

The plan of the paper is as follows. In section 2 we give a general description of the numerical model and details of the applied forcing. Section 3 contains the results of the experiments and their interpretation, and a discussion with conclusions follows in section 4.

Section 2: General description of the numerical model and details of the applied forcing.

a)The model

The model of the stratosphere and mesosphere is global and is based on the primitive equations. The height of its lowest isobaric surface, 300 mb, can be prescribed and this allows departures from axially symmetric motion in the upper atmosphere to be forced from below. A full description of the model has been given by Butchart et al. 1982, although our version uses finite differencing accurate to fourth order rather than to second order. Summarising its main features, it has a regular grid in spherical co-ordinates with 16 points along a latitude circle, 36 points along a meridian from pole to pole and 33 levels at equal intervals of log(pressure), giving a vertical resolution of about 2.6 km. Radiative damping is represented by a simple Newtonian scheme with a time scale of about 20 days in the lower and middle stratosphere and about 5 days in the upper stratosphere and mesosphere. Holton's (1976) parametrisation of the drag due to the dissipation of waves is included as a Rayleigh friction 'sponge layer' at upper levels. This has only a small effect in the stratosphere which is the region of interest.

Integrations are initialised using global fields analysed from observational data of geopotential height and gradient winds. In the stratosphere, thicknesses between various isobaric levels are derived principally from radiance measurements by a stratospheric sounding unit (SSU) on the satellite NOAA-6. These thicknesses are tied to an

analysis of the 100mb surface which is made using conventional data by the National Meteorological Centre, Washington. The observational data extends up to 1mb, near the stratopause. The numerical experiments were conducted without access to data for the mesosphere, whose circulation was crudely represented by extending the observed data upwards using a vertical profile of static stability derived from climatology. The mesospheric levels are included in the model only as a device for keeping the model's 'rigid lid' away from the domain of interest. The influence of the mesosphere on lower levels should be limited by the strong radiative damping.

b) The experiments and the applied forcing.

The experiments that we report here have been conducted using as an initial flow the zonally averaged state of the upper troposphere and stratosphere on 19 January, 1982. The field at the lower boundary, 300 mb, was the appropriate zonally averaged field of geopotential height taken from observations. To this was added an idealised growing perturbation in geopotential height, ϕ'_B, which has the following form

$$\phi'_B = A f(t) e^{-\theta^2/\alpha^2} \qquad (1)$$

where θ is the co-latitude from a co-ordinate pole placed at 45°N and 180°E. The constant α has a value of 15°. This value is chosen so that the perturbation has a horizontal scale comparable with

persistent troughs and blocking ridges in the troposphere. The function $f(t)$ has the form

$$f(t) = 1 - e^{-t/\tau} \tag{2}$$

where τ has a value of 5 days. The perturbation almost reaches full amplitude after 10 days and remains nearly steady thereafter. Three experiments were conducted with perturbations of small and large amplitude,

$$A = \begin{cases} \pm & 100 \text{ gpm} \\ - & 600 \text{ gpm} \end{cases} \tag{3}$$

The larger value is roughly the maximum deviation in geopotential height from its zonal mean value found in observations at 300 mb and occurs in the centre of intense blocking anticyclones or persistent troughs like the one over SE Asia. In emphasising a local view of the dynamics, we wish to avoid defining the perturbation response as a departure from the current zonal mean. Instead, a perturbation field is measured as an anomaly, viz.

$$\phi' = \phi - \phi_c \tag{4}$$

where ϕ is the value in the perturbation experiment and ϕ_c is the corresponding value in a control run without the disturbance ϕ'_B at the lower boundary. All fields ϕ_c are independent of longitude, but

change slowly with time in the stratosphere because of the parametrised frictional drag and radiative relaxation included in the model.

The purpose of the small-amplitude experiments is to demonstrate the structure and propagation of disturbances to which linear theory should be closely applicable over most of the atmospheric domain. We test for linearity by changing the sign of A and noting whether ϕ' changes sign accordingly. Even for small $|A|$ it is necessary to test the experiments for linearity because we employ a fully non-linear model. We find that the linear approximation for small $|A|$ is good except in the vicinity of a 'critical region' which forms near a zero-wind line but remains narrow latitudinally for the duration of the experiments.

The purpose of the large-amplitude experiment is to show how non-linear processes occurring locally affect the evolution of ϕ when perturbations are as strong as those found in the real atmosphere. This is done by comparison with a small-amplitude experiment, and is facilitated by scaling the perturbation fields in the latter experiment by a factor of 6. The scaled fields are then approximately the formal linear response to forcing with $A = \pm 600$ gpm, except in the narrow critical zone referred to above.

A fundamental reason why the scaled 'linear' and the fully non-linear perturbation fields differ is that potential vorticity is not conserved for the former, and the limitations of linear theory are exposed where the constraint imposed by conservation is seriously broken.

Section 3: Results

In this section we present the results of the small and large amplitude perturbation experiments on the zonally averaged state of the atmosphere for 19 January 1982. Perturbation fields are supplemented for the large-amplitude experiment by isentropic maps of Ertel's potential vorticity, Q (for a definition see Gill 1982). We take the movement of contours of constant Q as indicating that of material lines over periods of a week or so which are short compared with the radiative damping time. However, where small scales of motion are generated in the large-amplitude experiment, the Q contours cannot be expected to represent material lines in detail because of truncation in the gridpoint model.

Figure 1 shows the zonal mean winds for the northern hemisphere for 19 January 1982. It comprises a tight westerly jet at high latitudes with easterlies extending to middle latitudes at mid-stratospheric levels. Fig.2 shows the associated distribution of Q on the 850 K isentropic surface (near 10 mb, about 30 km) along with wind vectors on the same surface. For our case Q decreases monotonically from the pole to middle latitudes where there is a band where the meridional gradient is weakly reversed (shaded in the figure). The zero-wind contour, as marked by the dashed line, is embedded in this region of reversed gradient, a point which should be noted for our later interpretation of results. Where winds are westerly, linear theory predicts that stationary Rossby waves can only propagate in regions where Q increases towards the pole. This is readily inferred from the dispersion relation for such waves (Holton

1979). We therefore expect the reversed gradient of Q in mid latitudes to act as a barrier to the meridional propagation of disturbances, confining them to higher latitudes.

a) Small-amplitude experiments

The (scaled) perturbation response to a localised 'low' of amplitude 100 gpm is shown as a longitude-height section in Fig.3 . It is taken at 62.5°N which lies near the latitude where the stratospheric winds and the perturbation amplitudes are strongest. After 11 days of integration when the applied forcing has almost reached maximum amplitude, a Rossby wavetrain of 'highs' and 'lows' can be seen extending upwards and downstream from the forcing centred at 180°E. The perturbation has almost wrapped around the latitude circle and a high is building near 60°W, upstream and above the forcing at this latitude. By day 16, Fig.4 shows that this feature has developed further and that interference effects are occurring. Fig. 5 is a polar-stereographic map at 8 mb on day 16. The highs and lows are centred approximately on the 62.5°N latitude circle showing that the forcing has excited a perturbation which has propagated predominantly downstream as though it were confined to a channel north of the reversed gradient of Q, as we anticipated earlier. Notice that the zero contours separating the main low from the two main highs run along meridians at high latitudes, while at mid latitudes there is a region where these contours have a SE to NW orientation.

We investigate whether the response is linear by changing the

sign of the applied forcing. The polar-stereographic chart corresponding to Fig.5 is shown in Fig.6. The patterns at middle and high latitudes are strikingly similar in these figures, and apart from a change in sign there is good quantitative agreement between the two fields. At latitudes south of 45^{o}N where the perturbation response is weak, there are greater differences between the two fields. This is not unexpected in that, at this level, the zero-wind line extends almost to this latitude and would act as a critical line for a stationary wave perturbation. As the integration proceeds, non-linearities in the vicinity of the initial zero-wind line become increasingly important as the latitudinal width of this non-linear region increases (Warn and Warn 1978). Since the amplitude of the forcing is small, and because of damping in the model (both radiative and numerical), this critical region does not become wide during the period of the present integration. This is in marked contrast to the situation for large-amplitude forcing as discussed later.

By day 29 interference effects as the wavetrain wraps around the hemisphere are almost complete and the perturbation is now only slowly varying in time. Fig. 7 shows that the perturbation consists of a single high and low around a latitude circle, and that the largest zonal harmonic is that of wavenumber 1. Since the applied lower boundary perturbation has approximately equal amplitudes in zonal waves 1 and 2, the dominance of wave 1 in the steady state is in line with the linear calculations of Charney and Drazin (1961). They showed that for steady waves the westerly winds in the winter stratosphere favour the vertical propagation of zonal wavenumber 1 compared with waves of larger wavenumber. The larger wavenumber 2

response indicated for an earlier stage of the integration in Fig.4 does not contradict this theoretical prediction because a steady state had not been achieved. Linear calculations based upon the WKB assumption (e.g. Karoly and Hoskins,1982) show that the vertical component of group velocity for an harmonic disturbance is proportional to its zonal wavenumber. The initial response in the middle and upper stratosphere is therefore primarily wavenumber 2 as wavenumbers 3 and above are confined to lower levels by the westerlies.

The latitudinal confinement of the perturbation at mid-stratospheric levels is clearly demonstrated by the distribution of Eliassen-Palm fluxes shown for day 6 in Fig.8. This figure also shows the 'divergence' of the fluxes, the quantity denoted as D_F by Edmon et al. (1981).For linear waves the EP fluxes can be interpreted as showing the direction of wave propagation. Regions where wave activity is building coincide with areas of convergence of the EP fluxes (see Eq. 2.1 and discussion in the paper by Edmon et al.). At middle and high latitudes of the middle stratosphere the EP fluxes point almost vertically upwards,consistent with the lack of meridional propagation inferred from Figs. 5 and 6. The main convergence is centred in mid latitudes. Knowing that for linear, steady, undamped waves D_F is zero (the so-called 'non-acceleration theorem'; Andrews and McIntyre,1976), the region of convergence can be connected firstly with transience as wave activity builds at the leading edge of the disturbance, and secondly with dissipation as the disturbance propagates away from its source. After the applied forcing has reached almost constant amplitude, the transient contribution to D_F

eventually diminishes although convergence due to dissipation remains. The convergence is found to decrease accordingly.

Figure 8 also shows that there is a region of divergence near $45^{\circ}N$ out of which EP arrows point both polewards and equatorwards. The region where the EP arrows are polewards coincides with the latitudinal band of reversed meridional gradient, shaded in Fig.2. The region of divergence is also in accord with linear theory, even though the zero-wind line passes through it, because at this stage of the integration the non-linearities are small. (This is confirmed by the counterpart of Fig.8 for forcing of opposite sign.) In the quasi-geostrophic approximation, the following expression holds for linear, undamped waves (see Edmon et al., op. cit.).

$$\frac{\partial}{\partial t}\left(\frac{1}{2}\,\overline{q'^2}/\bar{q}_y\right) + \nabla.\underline{F} = 0 \qquad (5)$$

where $\underline{F}$ is the EP flux, ∇ is $\left(\frac{\partial}{\partial y}, \frac{\partial}{\partial z}\right)$, q' is the departure of the quasi-geostrophic potential vorticity from its zonal mean value $\bar{q}$, and $\bar{q}_y$ is the meridional gradient of this mean. (Dissipation leads to convergence and is neglected for current purposes.) We expect the positive quantity $\overline{q'^2}$ to increase while the disturbance is growing, and (5) shows that this will be connected with convergence or divergence of $\underline{F}$ according as $\bar{q}_y$ is positive or negative. Within the resolution of the model, the divergence of $\underline{F}$ is consistent with a growing perturbation in a region where $\bar{q}_y$ is reversed. The poleward pointing EP arrows can be interpreted as an 'over-reflection' of the waves from the latitudinal barrier to propagation imposed by

the reversed gradient of potential vorticity. The region of divergence is confined in the vertical for the following reasons: at lower levels $\bar{q}_y$ is positive in the domain shown so that a growing disturbance corresponds to a convergence, not a divergence of $\underline{F}$. At upper levels the reversed gradient of potential vorticity is further south (near 20°N) and because the radiative damping is stronger and has been acting for a longer time, the reflected waves are much weaker. The EP fluxes are consequently directed equatorwards, up the gradient of 'refractive index' defined by $\bar{q}_y/u$ (see Matsuno,1970).

b) The large-amplitude experiment.

The perturbation response at 8 mb on day 16 for an applied low with amplitude 600 gpm is shown in Fig.9. Comparing this field with the (scaled) small-amplitude field in Fig.5, the first downstream high from the forcing at 180°E is slightly stronger for the large-amplitude case. Further downstream, however, the response is much weaker: the downstream low is less intense and the second downstream high of Fig.5 does not occur as a separate feature. Notice in Fig.9 that above,to the north and slightly upstream of the forcing at 180°E the perturbation is stronger than in Fig.5. This appears to be the result of non-linearity unconnected with the downstream signal. This may be inferred from a comparison of figures like Fig.5 and Fig.9 on previous days before the small-amplitude signal has had time to propagate far downstream.

By day 29 at 8 mb, Fig.10 shows that the main low (near 60°W) is

much weaker than the corresponding feature in Fig.9. Stretching westwards from this low at lower latitudes, there is a band where the height perturbation is negative. The weak anticyclone in Fig.9 at $0^{o}E,35^{o}N$ has developed and moved north-eastwards to high latitudes (Fig.10), so that geopotential height has increased almost everywhere at high latitudes, consistent with deceleration of the zonal mean winds.

The patterns of EP fluxes and D_F at day 6 are shown in Fig.11, and are strikingly similar to those shown for the small-amplitude experiment in Fig.8. D_F is roughly 36 times that shown in Fig.8. As D_F involves a product of perturbation amplitudes, we can conclude that the response to large-amplitude forcing is approximately linear at this stage, recalling the factor of 6 between the forcing amplitudes. Our earlier discussion of the divergence in mid latitudes and the 'over-reflection' of waves manifested in poleward EP fluxes therefore applies. The region of over-reflection subsequently disappears, however, although it remains a feature of the small-amplitude response. By day 16, Fig.12 shows that the region of divergence has been replaced by one of strong convergence with EP arrows directed equatorwards. In terms of the EP diagnostics, the region of over-reflection has become one in which net wave activity propagates equatorwards because the reflection mechanism no longer operates. The quantity D_F no longer varies between small and large amplitude experiments in proportion to the forcing-amplitude squared, and in this sense the linear approximation is no longer valid. Thus all statements of wave propagation based on diagnostics drawn from linear theory must be treated with caution.

To understand the differences between the large and small amplitude experiments, we turn to isentropic maps of Ertel's potential vorticity, Q. For adiabatic, inviscid conditions, lines of constant Q on isentropic surfaces are material lines of the fluid. In the model, radiative damping can be neglected when comparing maps of Q on days up to a week or so apart. The limited resolution of the present model is probably a more serious restriction to the interpretation of maps of Q, because of the non-conservation of Q due to loss of small scales through truncation in the model. Nevertheless, companion experiments with higher spatial resolution suggest that the maps presented should give an adequate picture of the movement of material lines.

Figure 13 shows the map of Q for day 6 on the 850 K isentropic surface (near 10 mb). The initial collar of locally high values of Q at mid latitudes (associated with the shaded region in Fig.2) is broken up. This is likely to have happened by a combination of the limited resolution of the model and instability of the zonal flow where the poleward gradient of Q is negative (Charney and Stern,1962). By day 11, Fig.14 shows that some of the remnants of this collar have combined into tongues connected with the region of high Q in the main westerly vortex. The orientation of these tongues is from the SE to the NW (there is a hint of this development in the previous Fig.13 near 180°E). In quasi-geostrophic theory, this orientation is consistent with the poleward EP fluxes shown in Fig.8. The tongues are absorbed into the main westerly vortex as time progresses. The feature at 60°E is at a later stage in this process, being closer to the longitude of the applied forcing at 180°E. By day 16 the tongues have been almost fully absorbed by the vortex, as shown in Fig.15.

Their contribution to poleward EP fluxes at mid latitudes is swamped by the formation of two distinct tongues of high Q which have a SW to NE orientation, corresponding in Fig.9 to equatorward EP fluxes. These new tongues arise in association with incursions of low Q to high latitudes as anticyclones develop in the perturbation height field (Fig. 9).

The extreme buckling of the contours shown by our sequence of maps of Q can be interpreted as wave breaking near a zero-wind or critical line (McIntyre and Palmer, 1983 and 1984; Clough et al., 1985). The evolution depends upon the initial distribution of Q. As interpreted by the EP diagnostics, the critical line in our case first behaves as an 'over-reflector' of waves (poleward EP fluxes and divergence). The region then becomes one with convergent, equatorward EP fluxes. In contrast a critical line initially imbedded in a positive gradient of Q immediately shows the latter characteristics, as demonstrated in our extended paper (see also Warn and Warn, 1978). The strongest convergence of the EP fluxes in Fig.12 coincides with the zone of wave breaking. Despite the non-linearities in this region and the resulting qualifications to the validity of linear theory, the inference that wave activity escapes to low latitudes during wave breaking is consistent with our earlier finding that the downstream signal on day 16 from the large-amplitude forcing is weaker than its scaled linear counterpart.

The critical zone widens as wave breaking continues. By day 29 Fig.16 shows that extreme buckling of Q contours has occurred across a wide range of latitudes, as regions of low Q penetrate polewards. Comparing this figure with Fig.10, the two highs in geopotential

height coincide with areas of low Q while the weaker lows are associated with a long band of high Q extending around lower latitudes. To the extent that Q is conserved in our model, the isentropic advection of Q has led to a net increase of high Q at low latitudes and low Q at high latitudes. This is consistent with the raising and lowering of the 8 mb isobaric surface in Fig.10.

The simulated behaviour of critical regions must be unrealistic in some respects because not all small scales of motion generated in the real atmosphere will be resolved. Experiments are being conducted to study the evolution of critical regions for models of varying resolution, and the results will be reported in the extended paper.

Section 4: Discussion and conclusions.

In this paper, we examine the effect of localised disturbances in the troposphere on the circulation of the stratosphere. Rossby wavetrains are generated which propagate upwards and downstream in the middle atmosphere. Two types of experiment are conducted for a zonally averaged state of the winter stratosphere obtained using observatonal data. In one pair of experiments the forcing in the troposphere is of small amplitude and in the other it is of large amplitude. These experiments are compared to determine how non-linear processes affect the perturbation fields. This is done locally by defining the perturbation response to the forcing as an anomaly,i.e. as a departure from the response in a control experiment in which no asymmetric forcing was applied at the lower boundary of the model.

The meridional distribution of potential vorticity, Q, in the basic state influences the propagation of Rossby wavetrains of small amplitude. In particular, a region where the meridional gradient of Q is negative at mid latitudes in the stratosphere acts as an 'over-reflecting' barrier, confining the wavetrain to higher latitudes as though the perturbation were propagating downstream in a channel. This interpretation is made from fields of the Eliassen-Palm fluxes and their divergence. The use of linear arguments is justified by noting that the perturbation response changes sign over most of the domain studied when the sign of the forcing is altered. Non-linearities in the vicinity of the zero-wind line are confined meridionally owing to the smallness of the perturbation amplitudes. At higher levels, it is proposed that radiative damping inhibits the

formation of a reflected wave, and consequently the meridional propagation of the wavetrain is equatorwards.

The properties of the large-amplitude wavetrain cannot be explained beyond a certain time using linear theory. Rather the phenomenon of 'wave breaking' is exhibited by the extreme and irreversible buckling of contours of Q on an isentropic surface. Wave breaking occurs about the initial location of the zero-wind line, and is an inherently non-linear phenomenon (McIntyre and Palmer, 1983 and 1984).

In our case, the evolution of wave breaking is determined by the fact that the zero-wind line is initially embedded in a region where the meridional gradient of Q is negative. According to the EP fluxes and their divergence, the evolution begins with an 'over-reflecting' stage which is followed by one in which wave activity can propagate to low latitudes as perturbation amplitudes increase. It is suggested that this eventual equatorward 'escape' of wave activity due to wave breaking inhibits the downstream propagation of the disturbance.

A feature of the breaking regions revealed by our maps of Q is that they widen considerably with time. This is in accord with a key prediction of theories of critical regions which take their full non-linear nature into account (Killworth and McIntyre,1985). These broad regions of non-linearity mean that we must treat with caution conclusions made using diagnostics taken from linear theory. An examination of isentropic maps of Ertel's potential vorticity is therefore recommended before inferences about wave propagation are made.

References

Andrews D and McIntyre M [1976] Planetary waves in horizontal and vertical shear: the generalised Eliassen-Palm relation and the mean zonal acceleration. J.Atmos.Sci.,33,2031-2048.

Butchart N, Clough S, Palmer T and Trevelyan P [1982] Simulations of an observed stratospheric warming with quasigeostrophic refractive index as a model diagnostic. Q.J.Roy.Met.Soc., 108,475-502.

Charney J and Drazin P [1961] Propagation of planetary-scale disturbances from the lower into the upper atmosphere. J.Geophys.Res.66,83-109.

Charney J and Stern M [1962] On the stability of internal baroclinic jets in a rotating atmosphere. J.Atmos.Sci.,19,159-172.

Clough S,Grahame N and O´Neill A [1985] Potential vorticity in the stratosphere derived using data from satellites. To appear in the April 1985 edition of the Q.J.Roy.Met.Soc.

Edmon H, Hoskins B and McIntyre M [1980] Eliassen-Palm cross-sections for the troposphere. J.Atmos.Sci.,37,2600-2616.

Gill A[1982] Atmosphere-ocean dynamics. Vol.30 of the International Geophysics series. Academic Press.

Hayashi Y [1981] Vertical-zonal propagation of a stationary planetary wave packet. J.Atmos.Sci.,38,1197-1205.

Holton J [1976] A semi-spectral numerical model for wave, mean-flow interactions in the stratosphere: applications to sudden stratospheric warmings. J.Atmos.Sci.,33,1639-1649.

Holton J [1979] An introduction to dynamical meteorology. Vol. 23 of the International Geophysics series. Second edition, Academic Press.

Karoly D and Hoskins B [1982] Three-dimensional propagation of planetary waves. J.Met.Soc.Jap.,60,1,109-122.

Killworth P and McIntyre M [1985] Do Rossby wave critical layers absorb,reflect or over-reflect? To be submitted to J.Fluid.Mech.

Matsuno T [1970] Vertical propagation of stationary planetary waves in the winter northern hemisphere. J.Atmos.Sci.,27,871-883.

McIntyre M [1982] How well do we understand the dynamics of stratospheric warmings? J.Met.Soc.Jap.,60,1,37-65.

McIntyre M and Palmer T [1983] Breaking planetary waves in the stratosphere. Nature,305,593-600.

McIntyre M and Palmer T [1984] The 'surf zone' in the stratosphere. J.Atmos.Terrest.Phys., 9,825-849. Hamburg symposium issue.

O'Neill A and Taylor B [1979] A study of the major stratospheric warming of 1976/77. Q.J.Roy.Met.Soc,105,71-92.

Warn T and Warn H [1976] On the development of a Rossby wave critical level. J.Atmos.Sci.,33,2021-2024.

Warn T and Warn H [1978] The evolution of a non-linear critical level. Stud.Appl.Math,59,37-71.

$

Figure captions

Fig.1 Cross-section of zonal mean wind (ms^{-1} with easterlies shaded) for the northern hemisphere on 19 January 1982. On this and other vertical sections, the height co-ordinate, Z ,is given by Z = Hln(1000/P) where P is the pressure in mb and H=6.95 km.

Fig.2 Polar-stereographic map of Ertel's potential vorticity, Q, and winds on the 850 K isentropic surface of the initial state shown in Fig.1. The units are 10^{-4}K $m^2 kg^{-1} s^{-1}$. The region where the poleward gradient of Q is negative is finely dotted and the dashed and dotted curve gives the location of the zero-wind line. In the above units, the contour interval is 0.2 between values 1 and 3, while the interval is 1 for values greater than 3. The frame surrounding the figure is tangential to latitude 20^{0}N.

Fig.3 Longitude height section at 62.5^{0}N of the perturbation field in geopotential height for day 11 of the experiment with a 'low' of amplitude 100 gpm at the lower boundary. The perturbation field is scaled by a factor of 6 for comparison with the experiment where the forcing has amplitude 600 gpm (see section 2 for discussion). The units are geopotential dekametres and negative values are shaded.

Fig.4 As for Fig.3 but on day 16.

Fig.5 As for Fig.4 but on a polar-stereographic map at 8 mb with no shading of negative values.

Fig.6 Polar-stereographic map at 8 mb of the perturbation in geopotential height on day 16 for the experiment with a 'high' of amplitude 100 gpm at the lower boundary. The field is scaled as in Figs.3,4 and 5. The units are geopotential dekametres.

Fig.7 As for Fig.3 but on day 29.

Fig.8 The direction of the Eliassen-Palm flux and its 'divergence' (see text) on day 6 for the experiment with a 'low' of amplitude 100 gpm at the lower boundary. Note that the divergence has not been scaled. Contours are drawn at intervals of 5×10^{-8} ms^{-2} with regions of positive values dotted.

Fig.9 Polar-stereographic map at 8 mb of the perturbation in geopotential height on day 16 for the experiment with a 'low' of 600 gpm at the lower boundary. The units are geopotential dekametres.

Fig.10 As for Fig.9 but on day 29.

Fig.11 The EP fluxes and their 'divergence' on day 6 for the experiment with a 'low' of amplitude 600 gpm at the lower boundary. Contours are drawn at intervals of 2×10^{-6} ms^{-2}. Regions of positive values are dotted.

Fig.12 As for Fig.11 but on day 16. Contours are now drawn at intervals of 10^{-5} ms^{-2}.

Fig.13 Polar-stereographic map of Ertel's potential vorticity, Q, and winds on the 850 K isentropic surface on day 6 for the experiment with a 'low' of 600 gpm at the lower boundary. Units and contour intervals as in Fig.2.

Fig.14 As for Fig.13 but on day 11.

Fig.15 As for Fig.13 but on day 16.

Fig.16 As for Fig.13 but on day 29

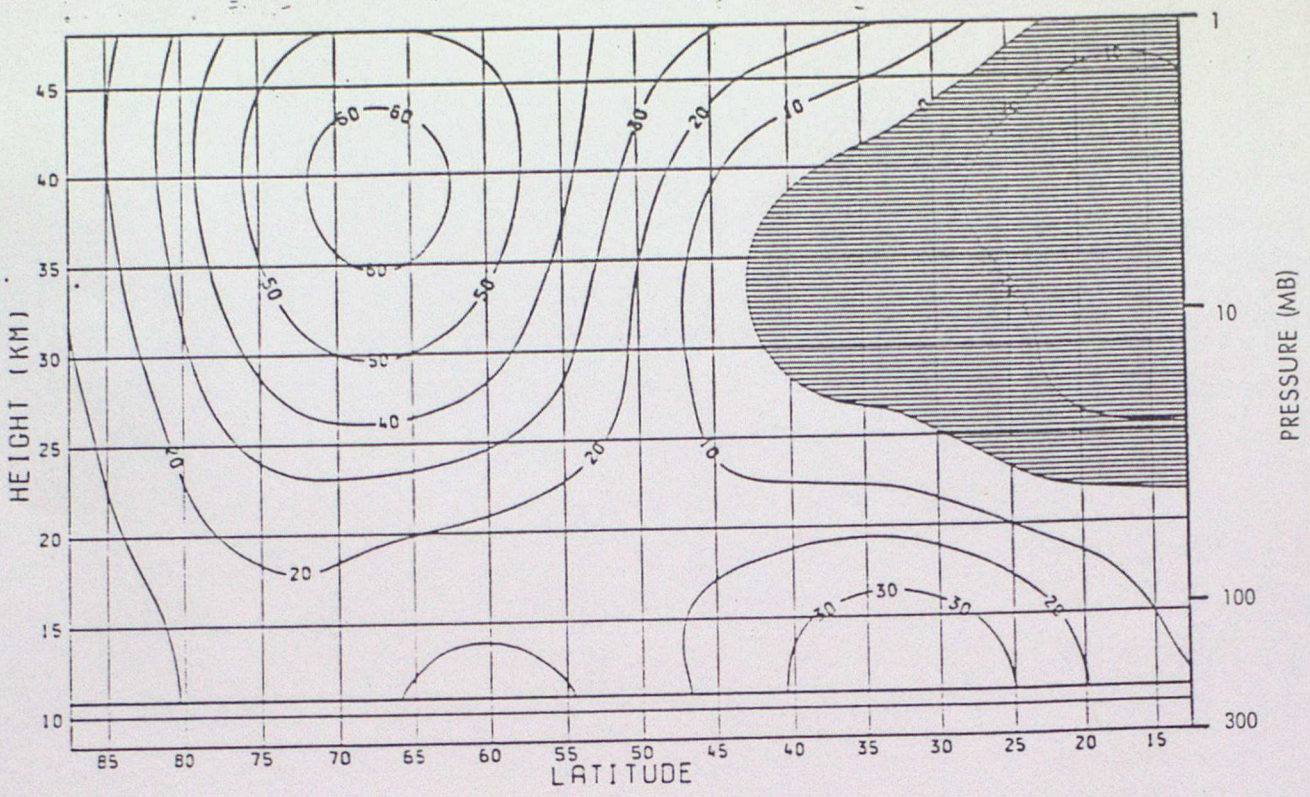
HEIGHT (KM)
45
40
35
30
25
20
15
10
85
80
75
70
65
60
55
50
45
40
35
30
25
20
15
LATITUDE
1
10
100
300
PRESSURE (MB)
60
50
40
30
20
10

fig. 1

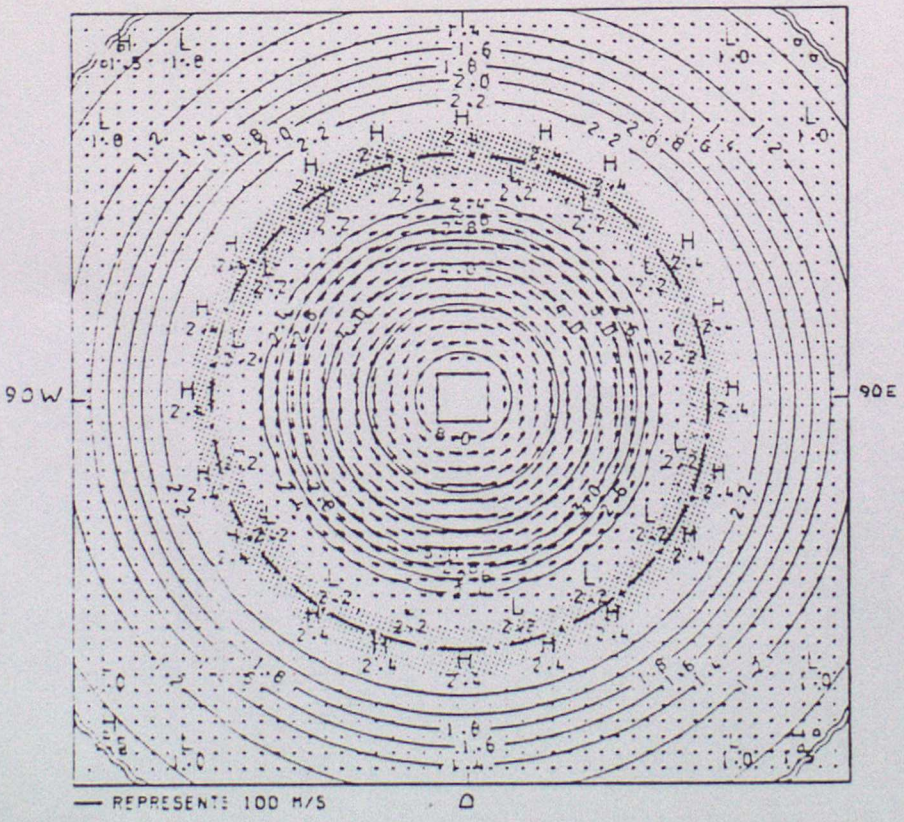
90W
90E
REPRESENTS 100 M/S

fig. 2

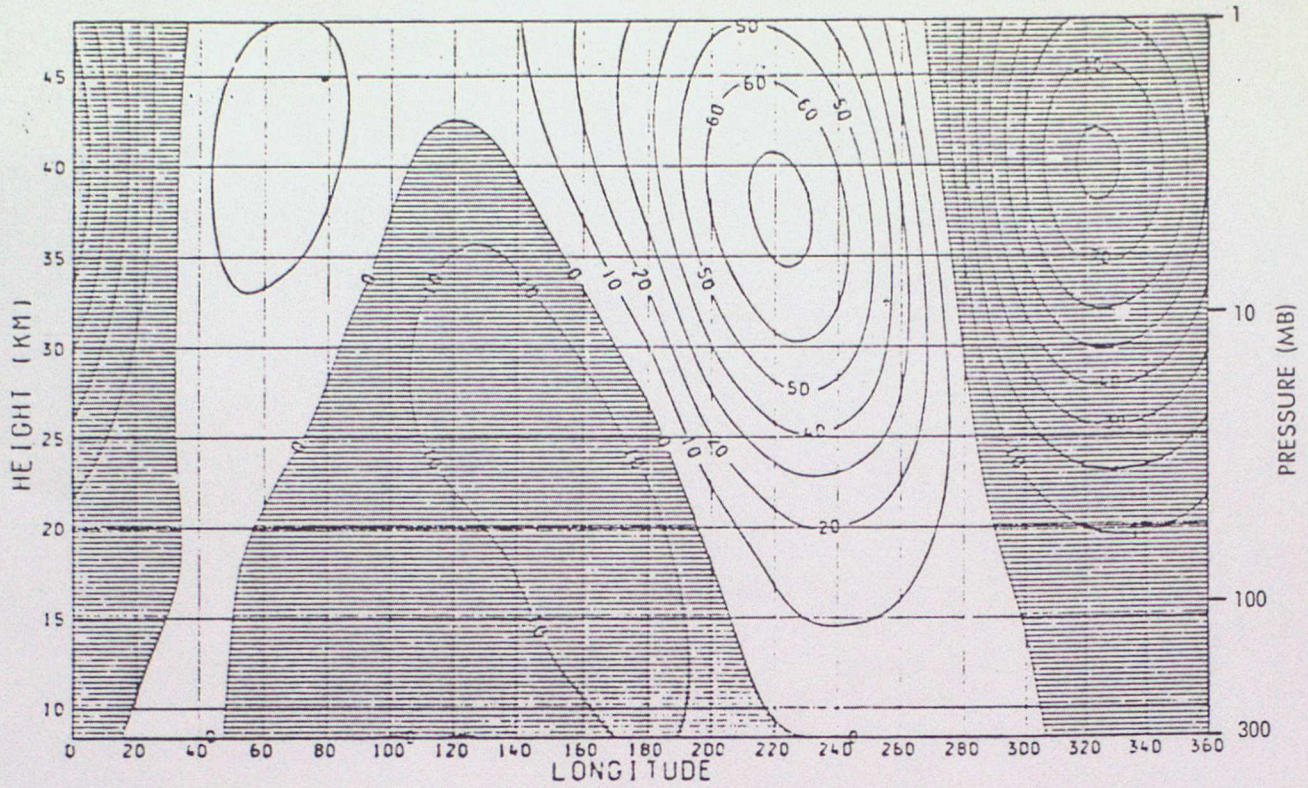
HEIGHT (KM)
PRESSURE (MB)
LONGITUDE
1
10
100
300
0 20 40 60 80 100 120 140 160 180 200 220 240 260 280 300 320 340 360
10 15 20 25 30 35 40 45

fig. 3

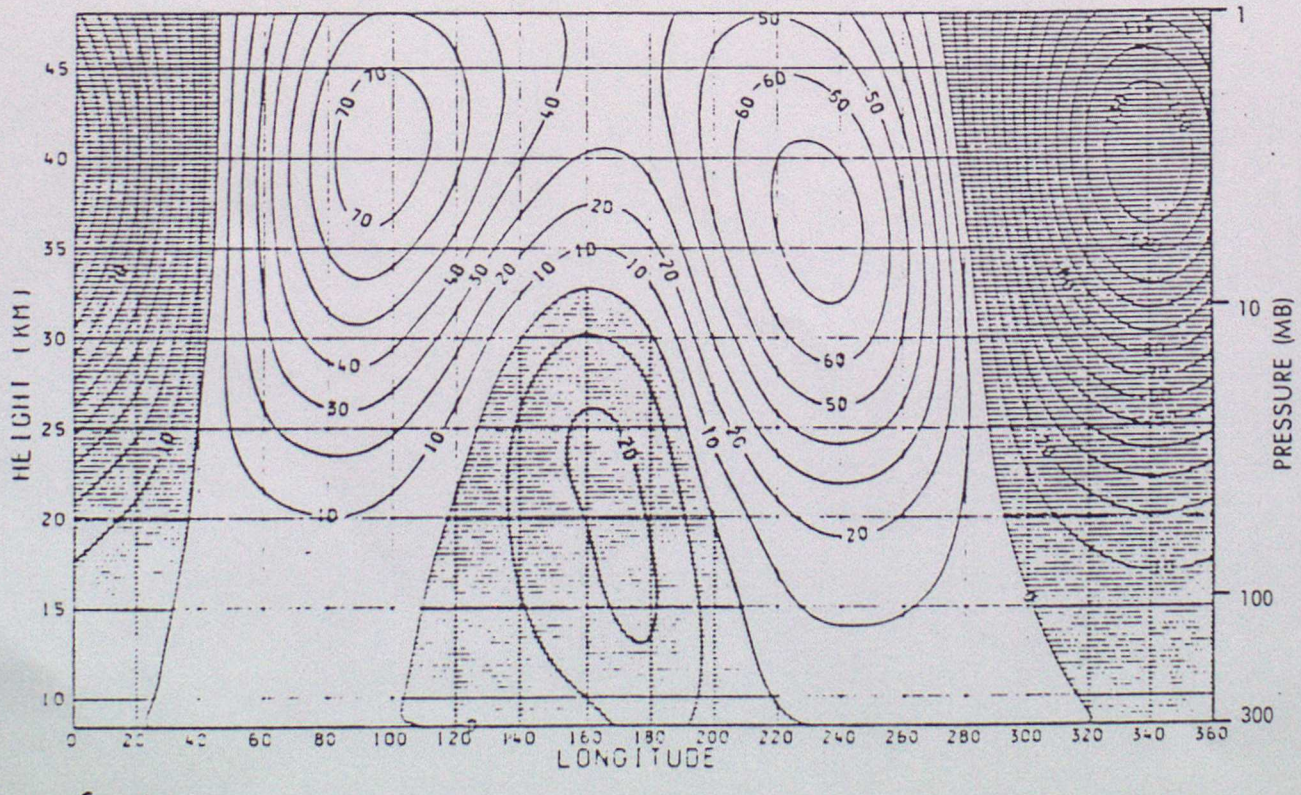
HEIGHT (KM)
PRESSURE (MB)
LONGITUDE
1
10
100
300
0 20 40 60 80 100 120 140 160 180 200 220 240 260 280 300 320 340 360
10 15 20 25 30 35 40 45

fig. 4

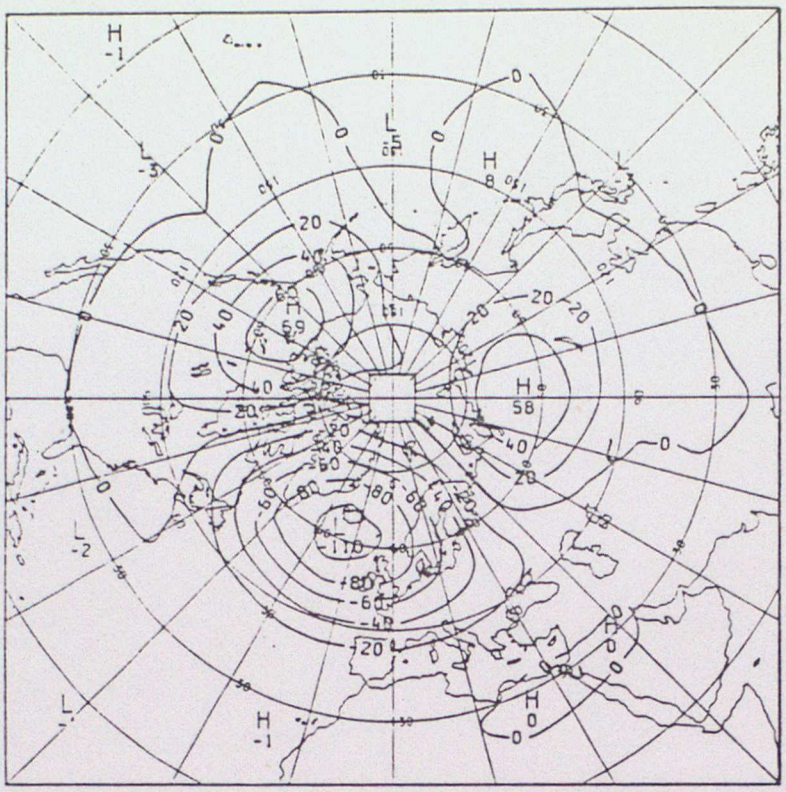

fig. 5

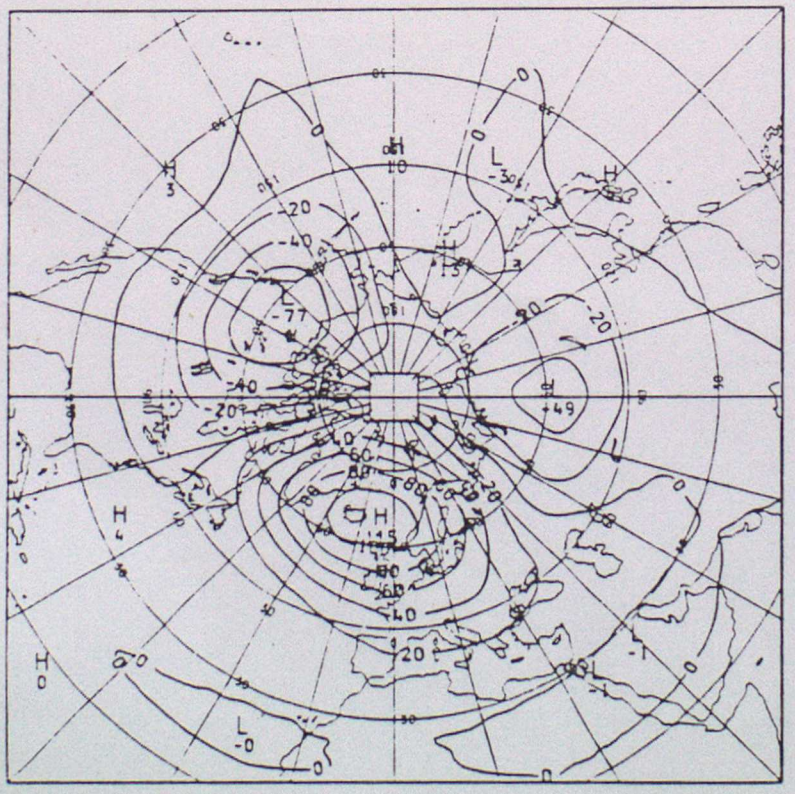

fig. 6

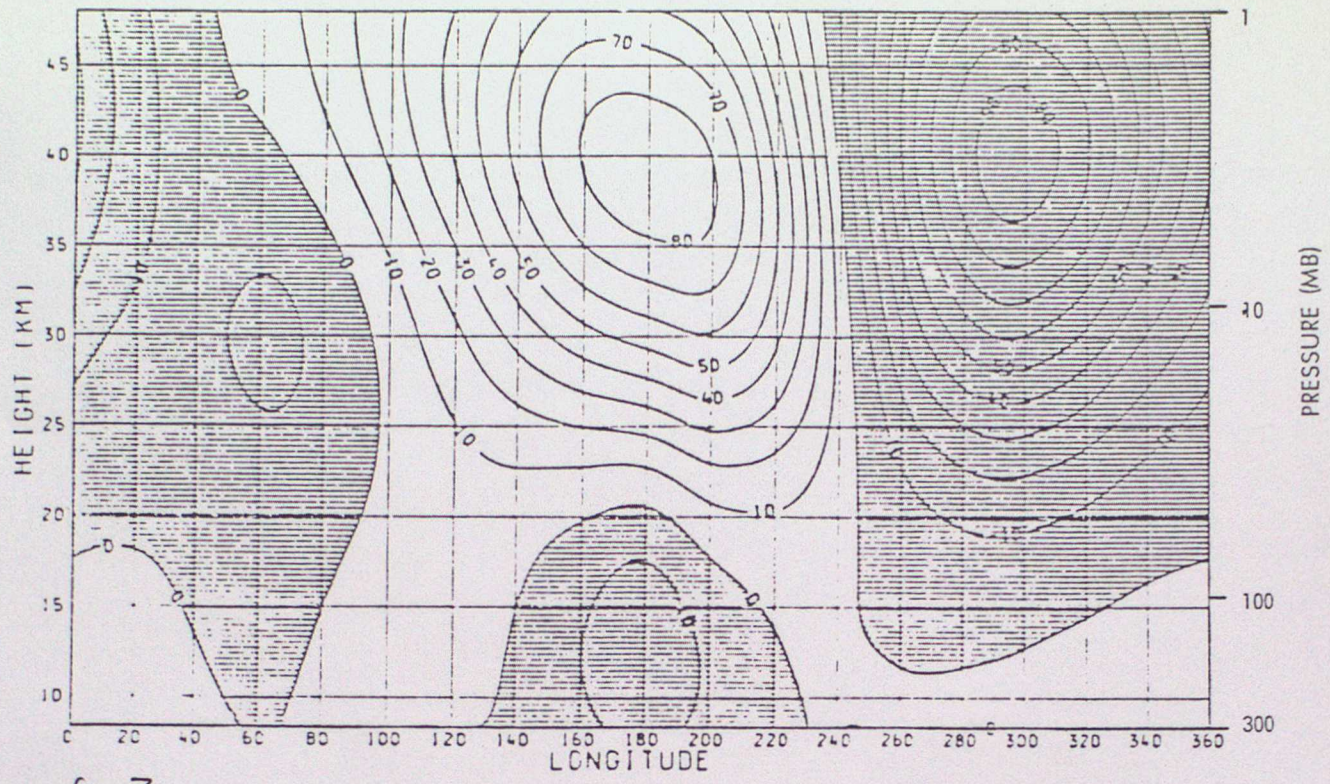
HEIGHT (KM)
LONGITUDE
PRESSURE (MB)
1
10
100
300
70
60
80
50
40
30
20
10
0
45
40
35
30
25
20
15
10
0 20 40 60 80 100 120 140 160 180 200 220 240 260 280 300 320 340 360

fig. 7

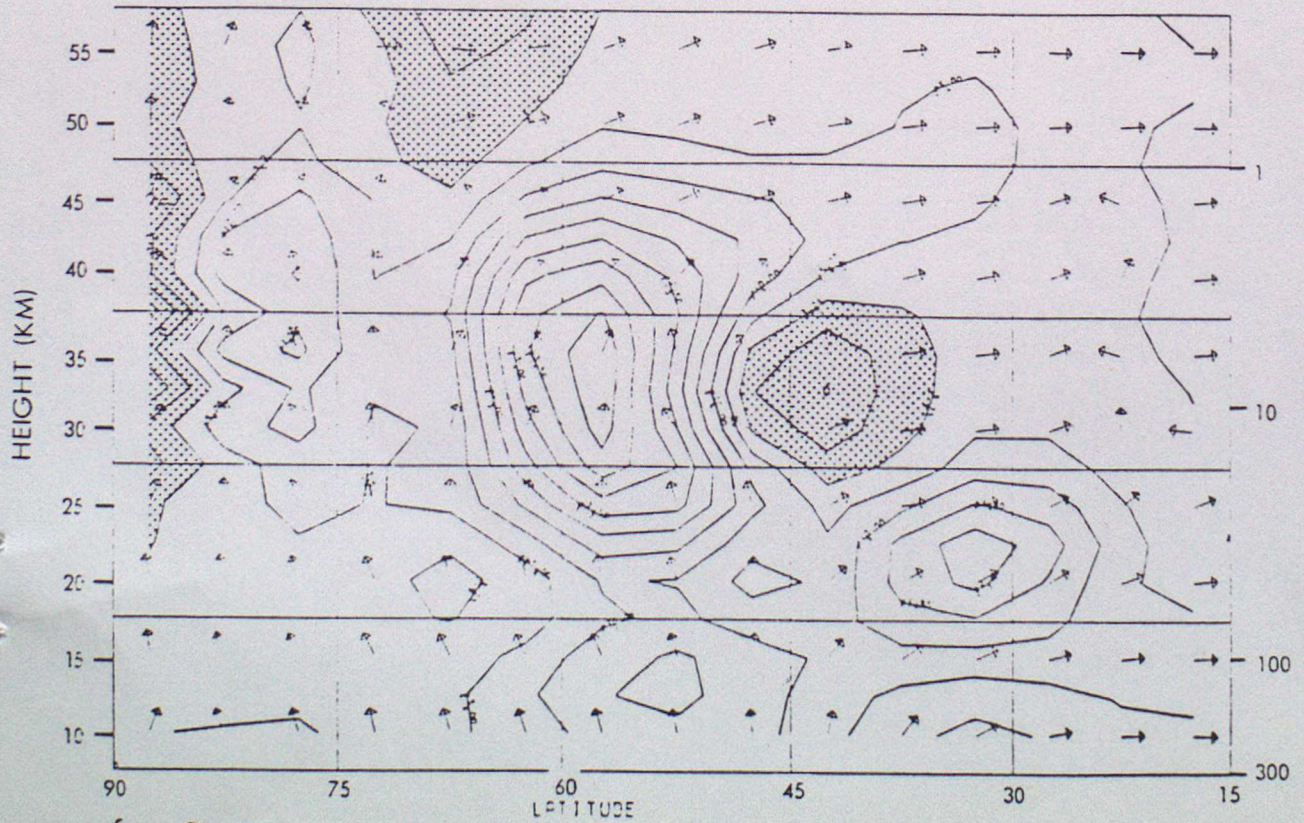
HEIGHT (KM)
LATITUDE
PRESSURE (MB)
1
10
100
300
55
50
45
40
35
30
25
20
15
10
90
75
60
45
30
15

fig. 8

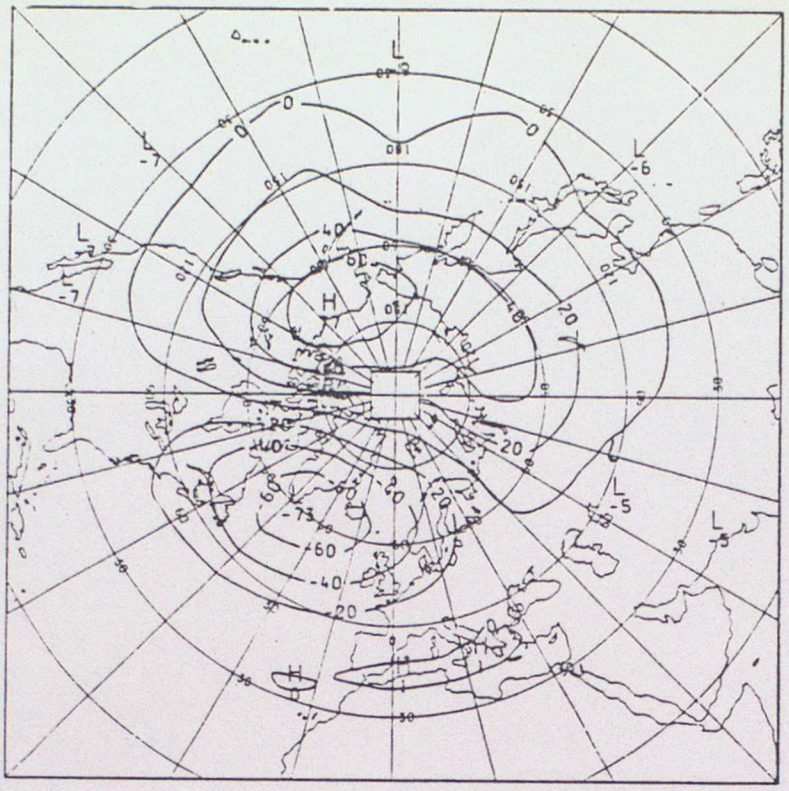

fig. 9

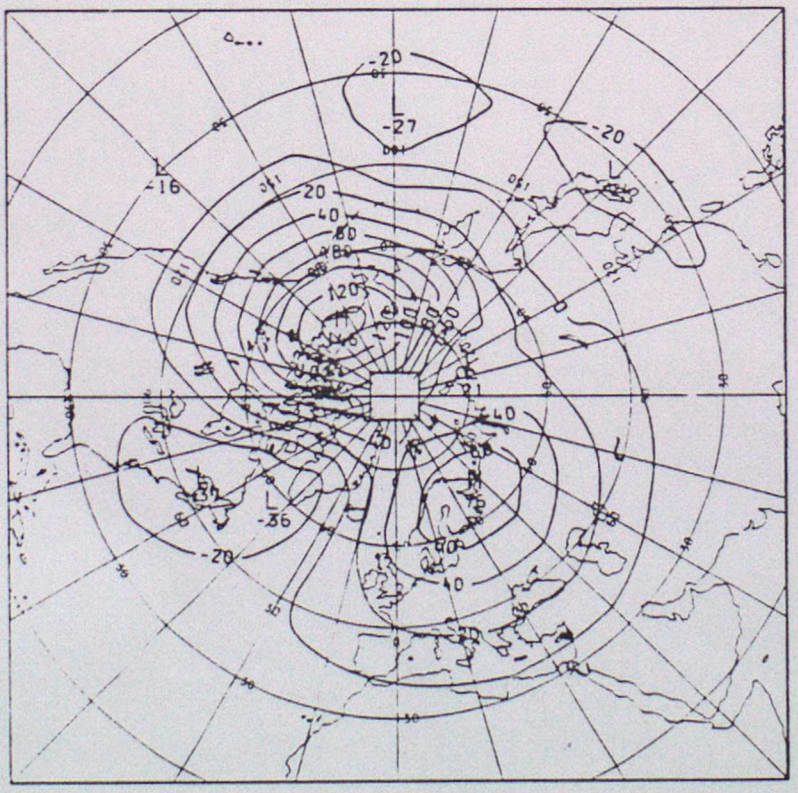

fig. 10

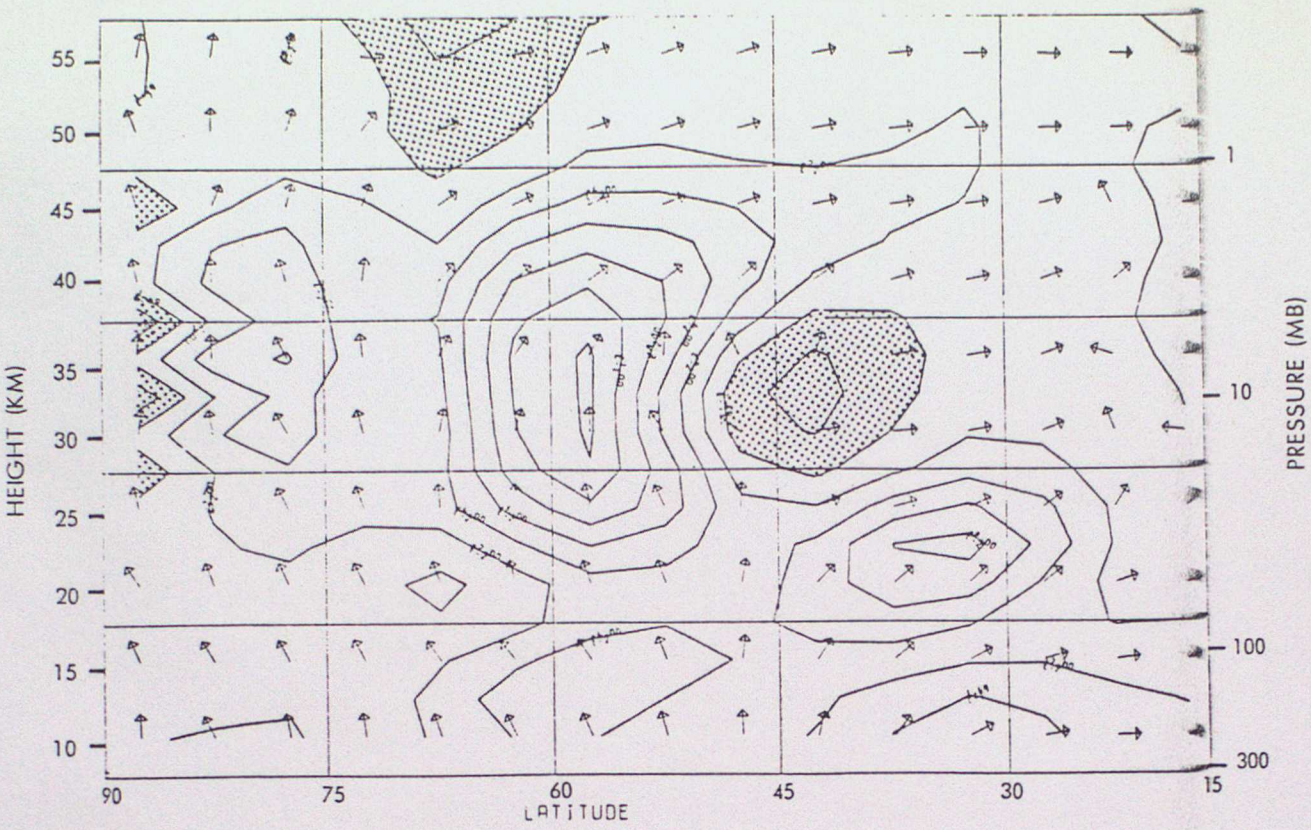
HEIGHT (KM)
55
50
45
40
35
30
25
20
15
10
90
75
60
45
30
15
LATITUDE
1
10
100
300
PRESSURE (MB)

fig. 11

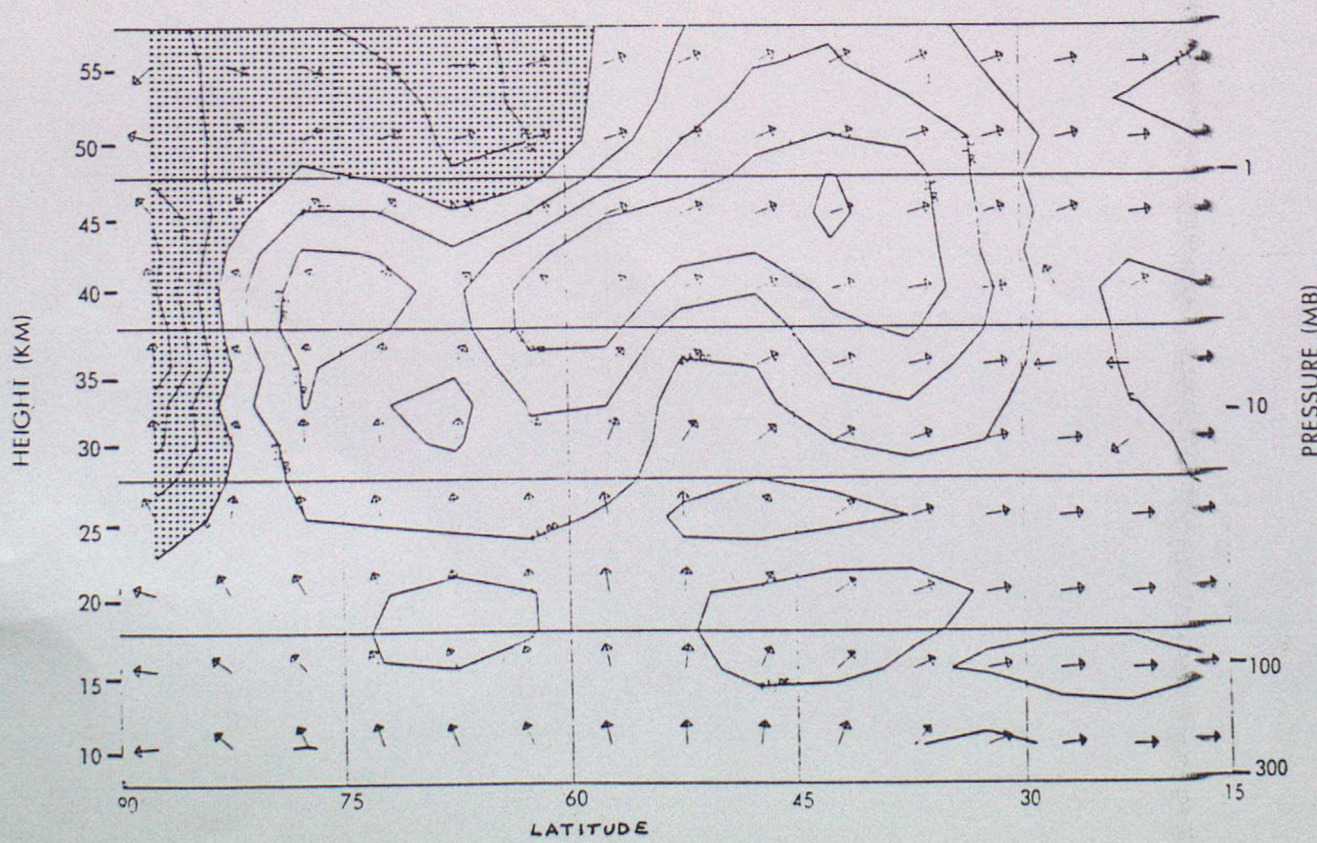
HEIGHT (KM)
55
50
45
40
35
30
25
20
15
10
90
75
60
45
30
15
LATITUDE
1
10
100
300
PRESSURE (MB)

fig. 12

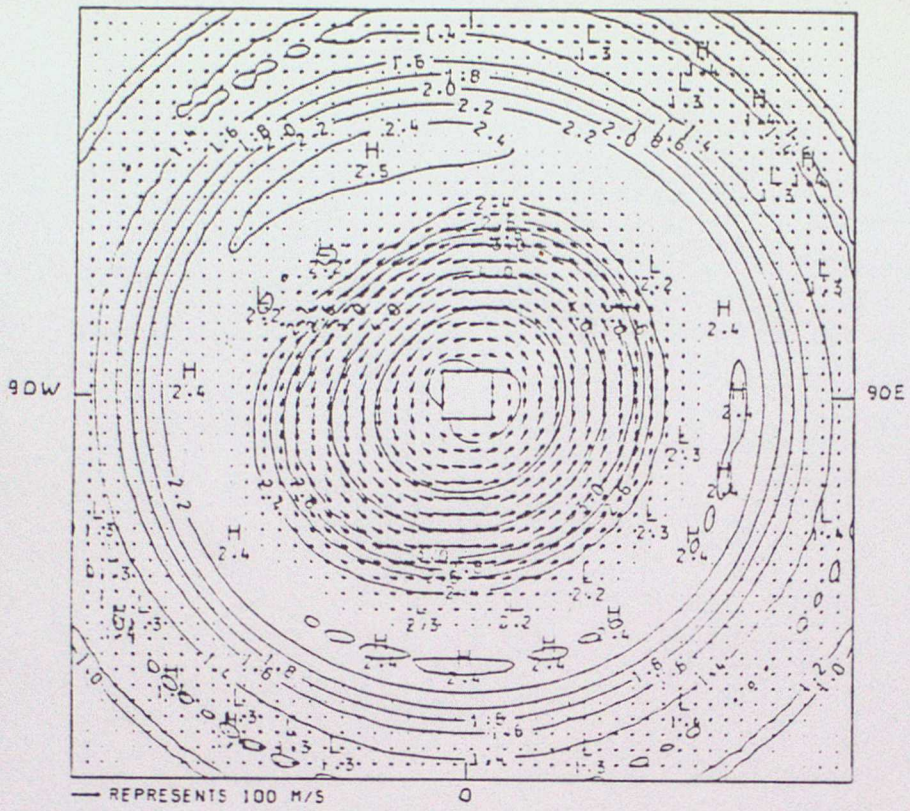

fig. 13

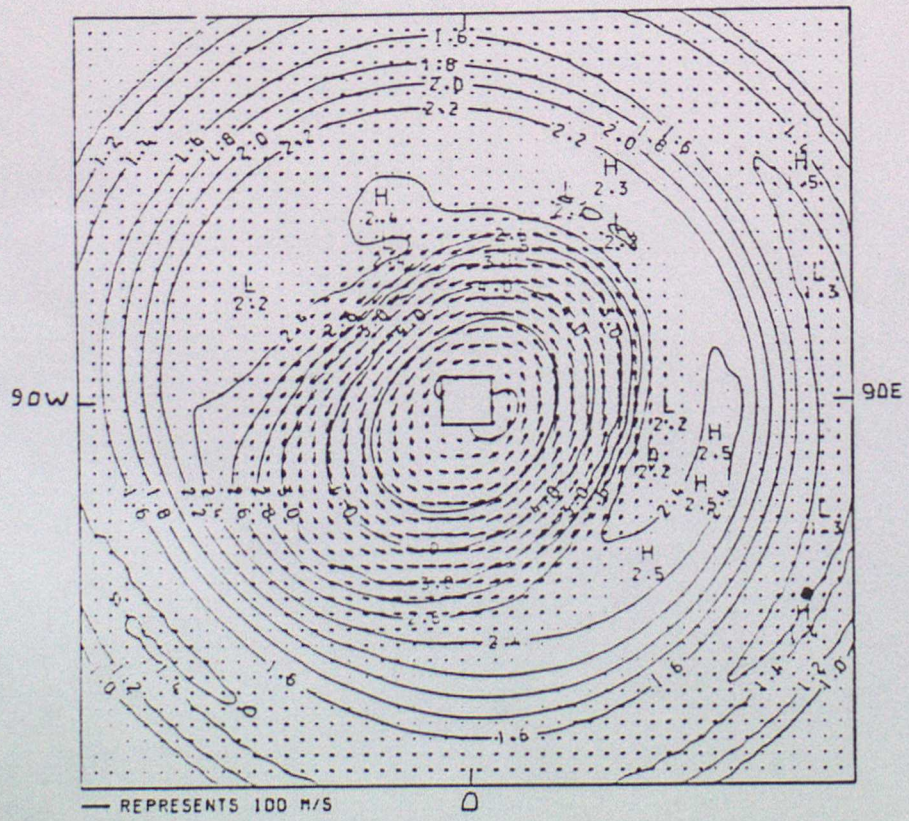

fig. 14

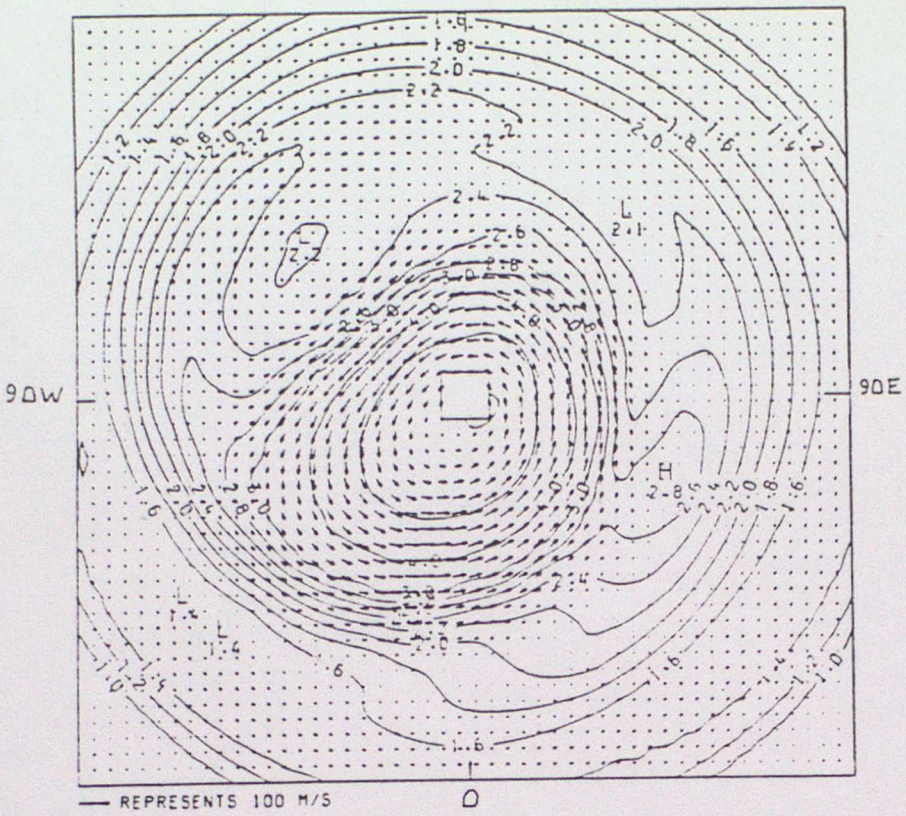

fig. 15

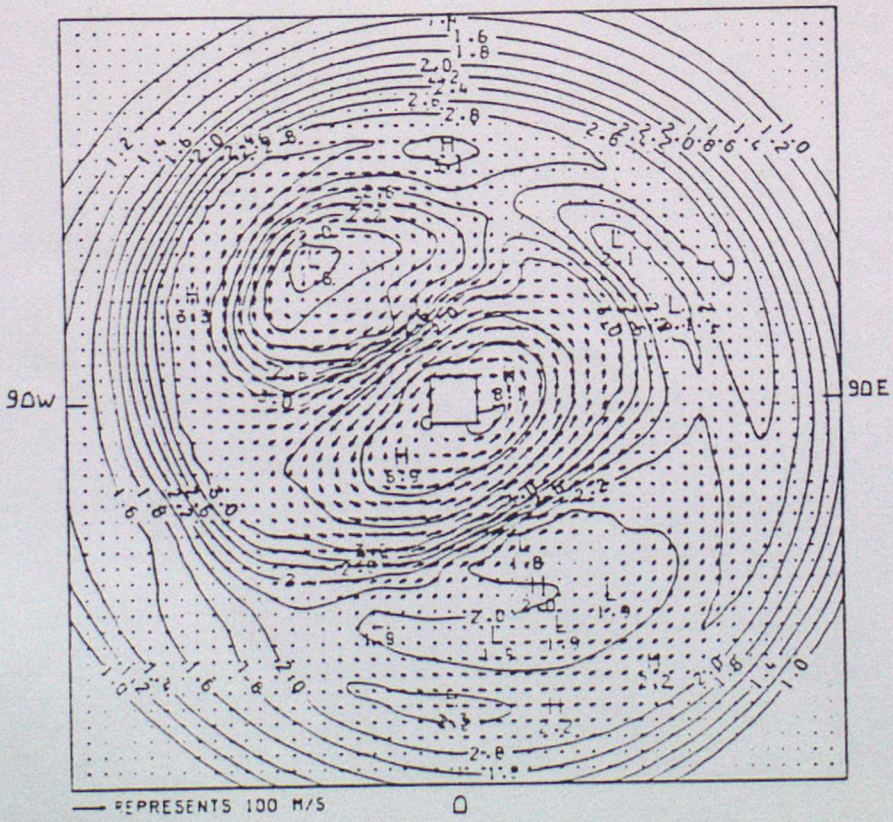

fig. 16